

The Chain Flexibility Effects on the Self-assembly of Diblock Copolymer in Thin Film

Mingyang Chen,^{1,2} Yuguo Chen,^{1,3} Yanyan Zhu,^{1,2} Ying Jiang,^{1,3,*} David Andelman,^{4,*} and Xingkun Man^{1,2,5,*}

¹*Center of Soft Matter Physics and its Applications,
Beihang University, Beijing 100191, China*

²*School of Physics, Beihang University, Beijing 100191, China*

³*School of Chemistry, Beihang University, Beijing 100191, China*

⁴*School of Physics and Astronomy, Tel Aviv University,
Ramat Aviv 69978, Tel Aviv, Israel*

⁵*Peng Huanwu Collaborative Center for Research and Education,
Beihang University, Beijing 100191, China*

Abstract

We investigate the effects of chain flexibility on the self-assembly behavior of symmetric diblock copolymers (BCPs) when they are confined as a thin film between two surfaces. Employing worm-like chain (WLC) self-consistent field theory, we study the relative stability of parallel (L_{\parallel}) and perpendicular (L_{\perp}) orientations of BCP lamellar phases, ranging in chain flexibility from flexible Gaussian chains to semi-flexible and rigid chains. For flat and neutral bounding surfaces (no surface preference for one of the two BCP components), the stability of the L_{\perp} lamellae increases with chain rigidity. When the top surface is flat and the bottom substrate is corrugated, increasing the surface roughness enhances the stability of the L_{\perp} lamellae for flexible Gaussian chains. However, an opposite behavior is observed for rigid chains, where the L_{\perp} stability decreases as the substrate roughness increases. We further show that as the substrate roughness increases, the critical value of the substrate preference, u^* , corresponding to an L_{\perp} -to- L_{\parallel} transition, decreases for rigid chains, while it increases for flexible Gaussian chains. Our results highlight the physical mechanism of tailoring the orientation of lamellar phases in thin-film setups. This is of importance, in particular, for short (semi-flexible or rigid) chains that are in high demand in emerging nanolithography and other industrial applications.

* yjiang@buaa.edu.cn; andelman@tauex.tau.ac.il; manxk@buaa.edu.cn

INTRODUCTION

With the growth of the microelectronic industry, small-size transistors with well-controlled nanostructures extending over large length scales are in high demand.¹ The self-assembly of block copolymers (BCPs) is considered a promising venue to meet these requirements.²⁻⁴ The simplest of all BCP architectures is the AB diblock copolymer (di-BCP), where each chain is composed of two chemically distinct blocks that are covalently tethered together. Di-BCPs can microphase separate to form a variety of equilibrium nanostructures such as lamellar and cylindrical phases.^{5,6} By tuning the BCP polymerization index N (or equivalently, the molecular weight)^{1,7} and the polymer chain rigidity *via* the choice of the chemical constituents for monomers (e.g, conjugated polymers^{8,9}), these spontaneously generated nanostructures have typical periodicities in the 5-100 nm range, which make them ideal for patterning technologies.¹⁰⁻¹²

A considerable amount of effort has been devoted to producing lamellae or cylinders of BCP thin-film of small domain size.¹³⁻¹⁶ Using a poly(styrene-*b*-dimethylsiloxane) (PS-PDMS) block copolymer with a total molar mass of 16 kg/mol ($N = 160$), Jung *et al.* reported¹³ formation of arrays of parallel cylinders with a periodicity of 17 nm. Later, a 6.4 kg/mol ($N = 63$) poly(styrene-*b*-4vinylpyridine) (PS-P4VP) block copolymer was used to obtain lamellae with a characteristic size of 10.3 nm.¹⁴ Deng *et al.* reported¹⁵ a low molar mass poly(pentadecafluorooctyl methacrylate)-*b*-polyhydroxystyrene (PPDFMA-PHS) ($N = 38$) forming nanodomains with a characteristic size of 9.8 nm. Recently, Xu *et al.* used¹⁶ poly(styrene-*b*-(4-vinylpyridine)propane-1-sulfonate) (PS-PVPS) with $N = 21$ to obtain a lamellar phase with a periodicity of 5.7 nm.

For these BCPs with high Flory-Huggins interaction parameter χ associated with a low degree of polymerization,¹⁷⁻²¹ the A/B constituent blocks usually have considerably different surface energies. However, for many materials and engineering applications, one has to rely on a thin-film set-up to produce BCP films with a perpendicular orientation of the BCP lamellae or cylinders with respect to the underlying substrate.¹² For example, in optoelectronic applications, controlling the orientation of the lamellar phase confined in a thin film has attracted considerable attention because the chain alignment is closely related to the efficiency of charge transport.^{9,10} Therefore, various techniques, such as solvent vapor annealing (SVA) and patterned substrates,²²⁻²⁴ have been developed to eliminate the surface

preference and to stabilize the perpendicular orientation (L_{\perp}).

Corrugated substrates are usually used to overcome such surface preference to obtain the perpendicular L_{\perp} phase.² Theoretical studies based on the self-consistent field theory (SCFT) indicate that the parameter $q_s R$ plays the key factor in inducing an L_{\parallel} -to- L_{\perp} phase transition,^{25,26} where q_s is the wavenumber and R is the amplitude of a sinusoidally corrugated substrate. In yet another work,²⁷ similar results were found for the orientation of cylindrical BCP thin films placed on top of a corrugated surface. Employing dissipative particle dynamics (DPD) simulation,²⁸ it was found that the BCP arrangement can induce an L_{\perp} perpendicular orientation of the higher layer BCP in a uniform multilayer nano-system. Furthermore, a phenomenological theory compared the L_{\parallel} and L_{\perp} free energies on corrugated substrates by using the analogy between smectic liquid crystals and lamellar BCP. The main finding was that by increasing the corrugation amplitude, the perpendicular lamellar (L_{\perp}) is the preferred phase.^{29–31} Such theoretical findings are consistent with experimental results.^{22,32–34}

Previous theoretical works have been focusing on the self-assembly of thin films of *flexible* chain BCPs. However, the above-mentioned short BCP chains and some other types of BCPs (like conjugated BCPs) whose semi-flexibility is particularly pronounced,^{8–10,35–37} no longer have the coiled conformation as was assumed in most previous theoretical works. Therefore, the flexible chain assumption based on the Gaussian chain (GSC) model is inappropriate to describe the chain statistics for polymers with a low degree of polymerization or chains that are not fully flexible.^{38,39} For such polymers, a more suitable model is the wormlike chain (WLC) model^{37,40} since it facilitates the study of the conformational variations of polymer chains, which deviates from the GSC model. A WLC is commonly used to describe a semiflexible polymer where the polymer appears rigid approximately within the persistence length λ . Thus, the polymer chain conformations can be quantified by the ratio L/λ , where L denotes the total contour length of a WLC. In the limit of $L/\lambda \gg 1$, the WLC model exactly recovers the GSC, where the effective Kuhn length is identified as $a = 2\lambda$ and L/a is equivalent to the degree of polymerization. On the other hand, for $L/\lambda \sim 1$ the WLC model crosses over and describes a rigid rod chain. Any finite L/a ratio in the WLC model gives rise to a theory that contributes to the effects of persistency on the phase behavior of AB diblock copolymer melts.

In our present study, we employ the WLC model that covers the entire range of chain

flexibility from Gaussian to semi-flexible and even rigid chains.^{17,41} Hence, it is appropriate to study also low L/a BCP systems. Herein, we use the self-consistent field theory (SCFT) based on WLC model^{18–21} for BCPs in a thin-film setup, with a top flat surface and a bottom corrugated substrate. We investigate the combined effects of the chain flexibility, the substrate roughness, and preference on the relative stability between the L_{\parallel} and L_{\perp} phases. Our findings show that the self-assembly behavior of rigid chains is *distinctively different* from Gaussian chains when the chains are cast on a corrugated substrate.

This paper is organized as follows. In the next section, we introduce the self-consistent field theory (SCFT) framework and the corresponding numerical schemes for solving the WLC-SCFT equations. In section III, we present our results and discussions, and section IV contains some concluding remarks.

MODEL

We outline the self-consistent field theory (SCFT) of the continuum worm-like chain model. Consider a semi-flexible polymer melt of n AB di-BCP chains confined between two surfaces. The total contour length for the entire BCP chain is L . Each BCP chain contains two linear blocks, fL is the contour length in the A block, and $(1-f)L$ in the B block, where f is the fraction of the A block. We concentrate on symmetric di-BCP, *i.e.*, $f = 0.5$. The persistence length λ , within which the orientational correlation between monomers decays exponentially, characterizes the polymer rigidity and is assumed to be the same for the A and B blocks, $\lambda = \lambda_A = \lambda_B$. The effective segment length a to be distinguished from the monomer size can be identified with twice the persistence $a = 2\lambda$ in a worm-like chain (WLC) model, and the parameter L/a becomes large for a flexible chain and small for a rod-like chain. Note that L/a is equivalent to the degree of polymerization N only in flexible chain limit ($L/a \gg 1$).¹⁷

In order to facilitate the numerical convergence, a masking method is used to model the surface confinement, where the impenetrable surfaces are replaced by a mask with a “wall” component.^{42,43} We use a local incompressibility condition $\phi_A(\mathbf{r}) + \phi_B(\mathbf{r}) + \phi_w(\mathbf{r}) = 1$, where ϕ_A and ϕ_B are the volume fractions of the A and B blocks. The third “wall” component fraction is ϕ_w , and the rigid wall is replaced by a compressible (“soft”) component characterized by an energetic penalty cost for local density deviations from the incompressibility

condition. Hence, the penalty term is written as

$$\zeta(\phi_p(\mathbf{r}) + \phi_w(\mathbf{r}) - 1)^2 \quad (1)$$

where $\phi_p(\mathbf{r}) = \phi_A(\mathbf{r}) + \phi_B(\mathbf{r})$ is the polymer volume fraction and ζ is the energy penalty parameter.

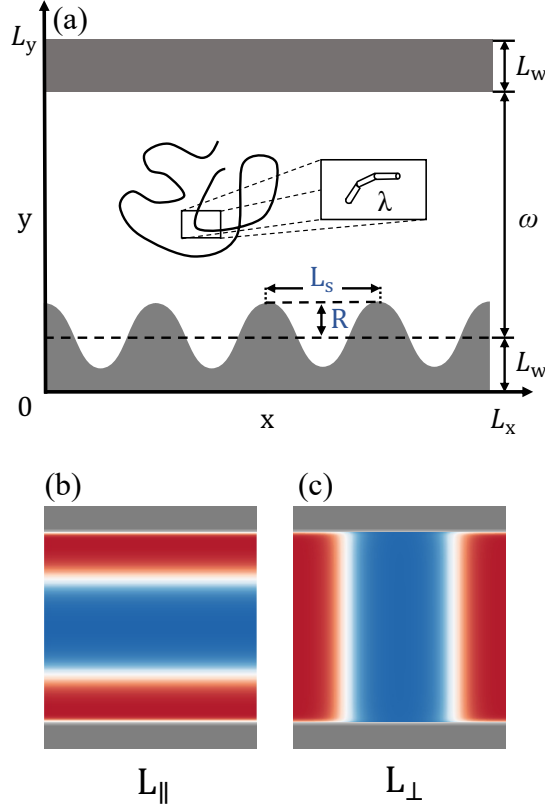


FIG. 1. Schematic illustration of a BCP film confined between a flat top surface and a sinusoidally corrugated bottom substrate. The persistence length of the semi-flexible BCP is λ . (a) The two-dimensional simulation box has the size $L_x \times L_y$, where $\omega = L_y - 2L_w$ is the averaged BCP film thickness and L_w is the average substrate height. The corrugated substrate is described by a height function: $h(x) = R \cos(2\pi x/L_s)$, with periodicity L_s and amplitude R . In (b), the lamellar orientation is parallel to the substrate (L_{\parallel}). In (c), the lamellar orientation is perpendicular to the substrate (L_{\perp}). A-rich regions are colored red and B-rich ones in blue.

The system is assumed to be translational invariant in the z -direction, so the numerical calculations are performed in an $L_x \times L_y$ two-dimensional box. With the above conventions, the Hamiltonian for a di-BCP film confined between two surfaces based on a WLC model

is written as:

$$\begin{aligned}
H[W_+, W_-] = C \int d^3\mathbf{r} & \left(\frac{[W_-(\mathbf{r})]^2}{\chi_{AB}(L/a)} - \frac{2u(L/a)}{\chi_{AB}(L/a)} \phi_w(\mathbf{r}) W_-(\mathbf{r}) \right. \\
& \left. + \frac{[W_+(\mathbf{r})]^2 - 2\zeta(L/a)\phi_p(\mathbf{r})iW_+(\mathbf{r})}{\chi_{AB}(L/a) + 2\zeta(L/a)} \right) \\
& - CV\bar{\phi} \ln Q[W_A, W_B]
\end{aligned} \tag{2}$$

where C is the normalization factor, and $\phi_p(\mathbf{r}) = \phi_A(\mathbf{r}) + \phi_B(\mathbf{r})$ is the polymer volume fraction. The Flory-Huggins interaction parameter between the A and B monomers is χ_{AB} , $u = (\chi_{wA} - \chi_{wB})L/a$ is the relative interaction between the substrate (w) and the A and B components, and χ_{wA} and χ_{wB} are the interaction parameters between the substrate and the A and B components, respectively. The polymer volume fraction averaged over the volume V is $\bar{\phi} = V^{-1} \int d^3\mathbf{r} \phi_p(\mathbf{r})$.

The quantity Q is the partition function of a single copolymer chain interacting with the two conjugate fields, $W_A = iW_+(\mathbf{r}) - W_-(\mathbf{r})$ and $W_B = iW_+(\mathbf{r}) + W_-(\mathbf{r})$. It can be calculated from the integral

$$Q = \frac{1}{4\pi V} \int d^3\mathbf{r} d^2\mathbf{u} q(\mathbf{r}, \mathbf{u}, s=1) \tag{3}$$

where the propagator $q(\mathbf{r}, \mathbf{u}, s)$ represents the probability of finding the s terminal, which is located in a spatial position specified by \mathbf{r} and points in a direction specified by the unit vector \mathbf{u} . Here, the propagator satisfies the modified diffusion equation (MDE)⁴⁴

$$\frac{\partial}{\partial s} q(\mathbf{r}, \mathbf{u}, s) = \left[\frac{L}{a} \nabla_{\mathbf{u}}^2 - L\mathbf{u} \cdot \nabla_{\mathbf{u}} - W(\mathbf{r}) \right] q(\mathbf{r}, \mathbf{u}, s) \tag{4}$$

The initial condition required for solving the MDE is $q(\mathbf{r}, \mathbf{u}, s=0) = 1$. In addition, for BCP, $W(\mathbf{r}) = W_A(\mathbf{r})$ for $0 \leq s < f$ (A block) and $W(\mathbf{r}) = W_B(\mathbf{r})$ for $f \leq s < 1$ (B block). A conjugated propagator, $q^*(\mathbf{r}, \mathbf{u}, s)$, can be defined and starts from the final terminal ($s=1$) where $q^*(\mathbf{r}, \mathbf{u}, s=1) = 1$. The $q^*(\mathbf{r}, \mathbf{u}, s)$ satisfies a similar MDE.

In the mean-field approximation, the thermodynamic properties of the confined BCP melt can be obtained from the saddle-point configuration of the free energy in eq 2, *i.e.*, solving

$$\frac{\delta H[W_+, W_-]}{\delta(iW_+(\mathbf{r}))} = \frac{\delta H[W_+, W_-]}{\delta(W_-(\mathbf{r}))} = 0 \tag{5}$$

The next step is to solve the MDEs for the two propagators $q(\mathbf{r}, \mathbf{u}, s)$ and $q^*(\mathbf{r}, \mathbf{u}, s)$, which depend on $\mathbf{r} = \mathbf{r}(x, y)$, the two-dimensional orientation vector \mathbf{u} , and the time-like

scalar variable s . A detailed formulation of the numerical procedure and its implementation in SCFT modeling of BCP systems can be found elsewhere.^{19,20,43,45,46}

The system setup is shown schematically in figure 1a. The “wall density”, ϕ_w , is fixed during the iterations. The flat top surface is characterized by a smoothly varying wall function:

$$\phi_w(y) = \frac{1}{2} + \frac{1}{2} \tanh \left[\frac{y - L_w - \omega}{\delta} \right] \quad (6)$$

where L_w and ω are defined in figure 1a, and δ is the interface width of the wall. The bottom sinusoidal substrate is described by a height function measured with respect to the average height:

$$h(x) = R \cos(2\pi x/L_s) \quad (7)$$

where R is the amplitude of the sinusoidal corrugation wall, and L_s is the corresponding periodicity. Thus, the bottom wall function is:

$$\phi_w(\mathbf{r}) = \frac{1}{2} - \frac{1}{2} \tanh \left[\frac{y - R \cos(2\pi x/L_s) - L_w}{\delta} \right] \quad (8)$$

The SCFT formulation gives the local density of the A and B components

$$\phi_A(\mathbf{r}) = \frac{\bar{\phi}}{4\pi Q} \int d^2\mathbf{u} \int_0^f ds q(\mathbf{r}, \mathbf{u}, s) q^*(\mathbf{r}, \mathbf{u}, s) \quad (9)$$

and

$$\phi_B(\mathbf{r}) = \frac{\bar{\phi}}{4\pi Q} \int d^2\mathbf{u} \int_f^1 ds q(\mathbf{r}, \mathbf{u}, s) q^*(\mathbf{r}, \mathbf{u}, s) \quad (10)$$

respectively. Therefore, there are two orientations of the lamellar phase with respect to the substrate, as shown schematically in figure 1. The parallel orientation (L_{\parallel} , figure 1b), and The perpendicular one (L_{\perp} , figure 1c).

The advantage of using such a WLC model is that the chain statistics changes continuously from Gaussian to semi-flexible and even to rigid chains as the L/a parameter changes from large values to small ones.^{17–21,40,41,47,48} In other words, the chain rigidity increases as the value of L/a decreases. In our work, we fix $\chi_{AB}L/a = 25$ and change L/a from 100 to 2 which implies that χ_{AB} changes from 0.25 to 12.5. In addition, the substrate roughness R and the surface preference u are changed in order to explore the relative stability of the L_{\perp} and L_{\parallel} phases. It is worth noticing that small values of the parameter L/a are practically meaningful for real polymer systems. According to experimental measurements, the value of L/a roughly ranges from 1 to 10 for conjugated block copolymers,^{8,49,50} block bottlebrush copolymers⁵¹ and liquid crystalline polymers.⁵²

RESULTS AND DISCUSSION

Varying the Chain Flexibility (L/a) for Flat Bounding Walls

We first discuss how varying the chain flexibility affects the relative stability of the parallel (L_{\parallel}) and the perpendicular (L_{\perp}) orientations, for BCP thin films, confined between two *flat and neutral* walls. The BCPs form a lamellar phase in the bulk with a periodicity $d_0 = d_0$ that is a function of the chain flexibility parameter, L/a . For flexible polymers ($L/a = 100$), the lamellar periodicity $d_0/a = 17.2$, is consistent with previous calculations based on the Gaussian model, $d_0 = 4.25R_g$ ($R_g = a\sqrt{N/6}$ is the chain radius of gyration). For chain flexibilities $L/a = 20, 10, 5, 3, 2$ and keeping a fixed, the obtained periodicities are, respectively, $d_0/a = 7.48, 5.07, 3.27, 2.25, 1.62$. The calculation box size for BCPs with different L/a is chosen according to their corresponding d_0 . In the following, the lateral size of the calculation box is fixed, $L_x = d_0$, for all calculations.

When the BCP film thickness, ω , deviates from an integer multiple of d_0 , the polymer chains in the L_{\parallel} phase will be stretched or compressed. This is seen in figure 2a from the free-energy difference $\Delta F = F_{\parallel} - F_{\perp}$ between the parallel free-energy, F_{\parallel} and the perpendicular one, F_{\perp} . Two significant features can be seen in figure 2a. (i) The free-energy difference ΔF has a local minimum when the film thickness ω equals the natural periodicity d_0 ; and, (ii) the free energy F_{\perp} is strictly lower than F_{\parallel} , and the value of the local minimum in ΔF varies for different L/a . The first feature can be understood because the residual elastic strains due to confinement will be suppressed when the film thickness equals an integer multiple of the natural periodicity d_0 .

To understand the second feature, we show the dependence of the ΔF local minimum on L/a in figure 2b. For rigid or semi-flexible chains ($L/a = 2, 3$ and 5), the local minimum of ΔF at film thickness $\omega/d_0 = 1$ increases as L/a decreases. When the polymer is fairly flexible ($L/a = 10, 20$, and 100), the local minimum of ΔF remains nearly unchanged. The inset in figure 2b shows the dependence on L/a of the entropy difference ΔS and enthalpy difference ΔU between the L_{\parallel} and L_{\perp} phases, respectively.

The numerical results indicate that the change of $\Delta F = \Delta U - T\Delta S$ is mainly caused by ΔS because ΔU remains nearly zero as L/a changes. In the calculations, the dimensionless

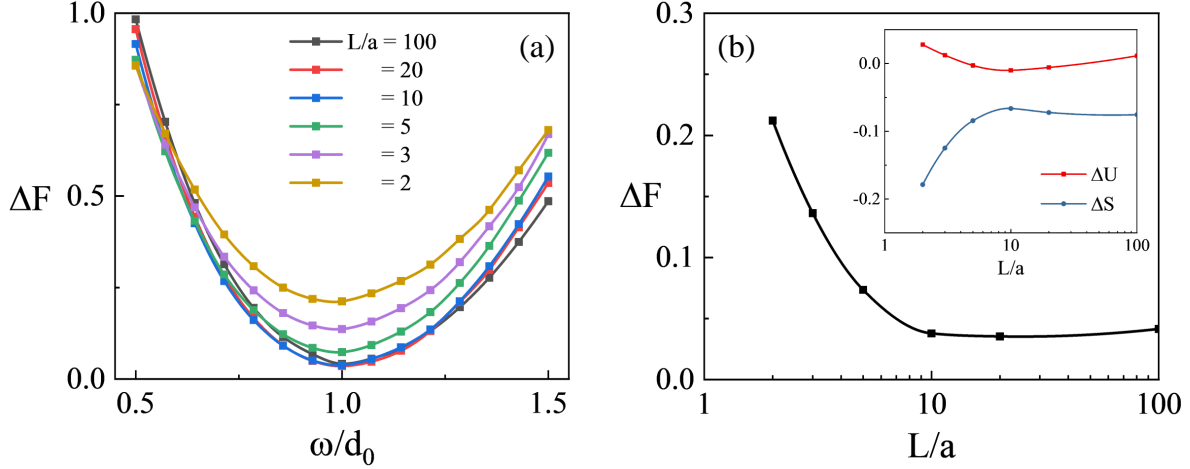


FIG. 2. (a) The free energy difference $\Delta F = F_{\parallel} - F_{\perp}$ between the L_{\parallel} and L_{\perp} orientations of BCP lamellar, in units of $nk_B T$, as a function of the film thickness, ω/d_0 , where n is the number of chains in the system, $k_B T$ is the thermal energy, and d_0 is the lamellar periodicity. The parallel free energy, F_{\parallel} , is calculated for one parallel lamella confined between two flat and neutral surfaces, with $u = R = 0$. The perpendicular free energy, F_{\perp} , corresponds to a perfect perpendicular lamellar phase. (b) Free energy (ΔF), enthalpy (ΔU) and entropy (ΔS) difference (inset) between the L_{\parallel} and L_{\perp} lamellar orientations, where $\Delta U = U_{\parallel} - U_{\perp}$, in units of $nk_B T$, and $\Delta S = S_{\parallel} - S_{\perp}$, in units of nk_B , as a function of the chain flexibility L/a . The other parameters are $L_x = \omega = d_0$ and $u = R = 0$.

entropy is

$$\frac{S}{nk_B} = \frac{1}{\bar{\phi}V} \int d^3\mathbf{r} (\phi_A W_A + \phi_B W_B) + \ln Q, \quad (11)$$

and the dimensionless enthalpy is

$$\frac{U}{nk_B T} = \frac{1}{\bar{\phi}V} \int d^3\mathbf{r} \chi_{AB}(L/a) \phi_A \phi_B. \quad (12)$$

Figure 2b indicates that the L_{\perp} phase is always more stable than L_{\parallel} . Moreover, the stability of L_{\perp} increases as L/a decreases. These results are consistent with previous studies,^{53,54} where it was shown that for two flat and neutral surfaces, the perpendicular orientation is favored over the parallel orientation because of the entropic confinement effect. This is the so-called “*nematic effect*” where a hard wall limits the chain conformations and facilitates the chain stretching along the substrate.^{17,55} Moreover, Pickett *et al.*⁵⁴ showed that the energy difference between the parallel and perpendicular orientations scales as $N^{-2/3}$. Therefore, ΔF increases as N decreases, which is also consistent with our full numerical calculations.

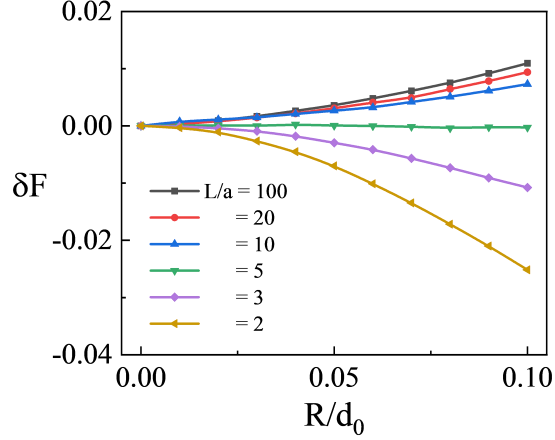


FIG. 3. Dependence of $\delta F = \Delta F(R) - \Delta F(R=0)$ on the amplitude R for different chain flexibility L/a , where the reference $\Delta F(R=0)$ is calculated for a flat ($R=0$) and neutral ($u=0$) substrate. Other parameters are $L_s = d_0$, $\omega = L_x = d_0$.

Substrate Roughness Effect

We investigate the combined effects of the wall roughness amplitude R and the BCP chain flexibility L/a on the relative stability between the L_{\parallel} and L_{\perp} phases. We fix the lateral size of the calculation box (L_x) and the corrugation periodicity (L_s), $L_x = L_s = d_0$, where $d_0 = d_0$ is a function of the L/a . We change the rescaled amplitude R/d_0 to obtain substrates with various roughness. It is clear that the order of magnitude of $\Delta F = F_{\parallel} - F_{\perp}$ is quite different for BCPs with different chain flexibility. Therefore, in order to compare the effect of R on the relative stability between the two lamellar phases for BCPs with different L/a , we analyze ΔF for each L/a by subtracting its corresponding free-energy difference for a flat substrate and the same L/a , $\delta F(R, L/a) = \Delta F(R, L/a) - \Delta F(R=0, L/a)$, indicating that L_{\perp} becomes more stable than L_{\parallel} as δF increases. It is worth noticing that for neutral surfaces, we obtain $\Delta F(R, L/a) > 0$ in all calculations. This result means that although the strength of relative stability between the two phases changes with R , the L_{\perp} phase is always more stable than the L_{\parallel} phase.

One of our main results is shown in figure 3 where we plot δF as a function of the roughness amplitude R for $L/a = 2, 3, 5, 10, 20$, and 100 . With the increase of the roughness amplitude R , δF manifests diverse variation tendencies for different chain flexibility, L/a . In the case of Gaussian chains ($L/a \geq 10$), δF increases as R increases. In the case of semi-

flexible polymer ($L/a=5$), δF remains nearly unaffected as R increases. However, for rigid chains, $L/a=2$ and 3, δF decreases with the increase of R .

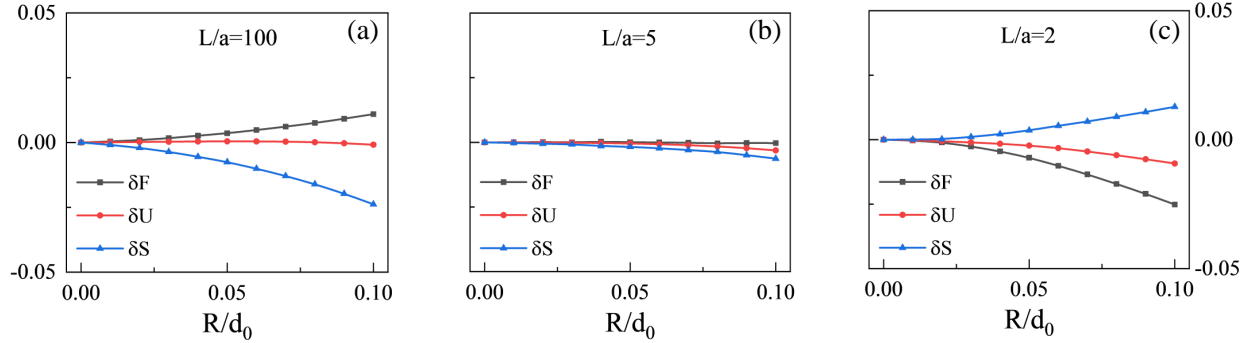


FIG. 4. Dependence of $\delta F = \Delta F(R) - \Delta F(R=0)$, $\delta U = \Delta U(R) - \Delta U(R=0)$, and $\delta S = \Delta S(R) - \Delta S(R=0)$ on the amplitude R for various chain flexibilities (a) $L/a = 100$, (b) $L/a = 5$, and (c) $L/a = 2$. ΔF , ΔU and ΔS are the same as in figure 2.

To understand these different trends, we analyze separately the enthalpy and entropy contributions to the free energy. Figure 4 shows the dependence of δF , δU and δS on R/d_0 for $L/a=2, 5$ and 100, separately. For each of these three quantities, we subtract their corresponding values for a flat substrate ($R=0$), as is defined in the caption of Figure 4, *i.e.*, $\delta F = \Delta F(R) - \Delta F(R=0)$.

Figure 4a shows the behavior for the Gaussian chain with $L/a=100$. With the increase of the rescaled amplitude R/d_0 , the entropy difference δS (blue line) decreases, while the enthalpy difference δU (red line) remains nearly unchanged. This can be understood in more detail by analyzing the chain configuration in the thin film geometry. Figure 5a shows the distribution of the chain ends for the L_{\parallel} phase on both flat and corrugated substrates. Our calculations show that the chain ends are evenly distributed in the entire thin film for a flat substrate. However, for corrugated substrates, the chain ends slide down into the valleys to accommodate the surface corrugations. In other words, the polymer chains are compressed due to the surface corrugation, indicating that increasing R leads to a decrease in chain configuration entropy of the L_{\parallel} phase. On the other hand, figure 5b shows that the chain end distribution for the L_{\perp} phase on a corrugated substrate is nearly unchanged as compared to a flat substrate. The reason for this difference in behavior is that the polymer chains are flexible and lie down in the L_{\perp} phase, as they can adjust easily to the surface corrugation. The outcome of these two different chain responses is that the decrease of S_{\parallel} is

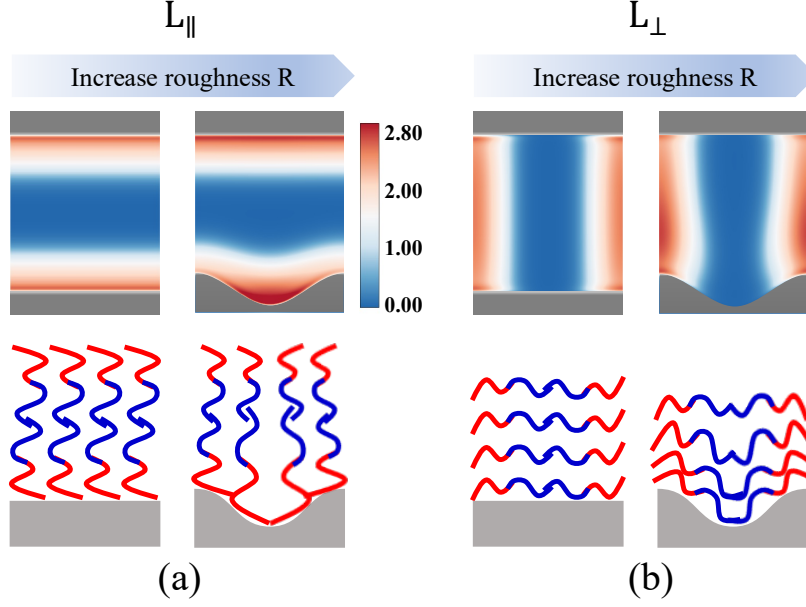


FIG. 5. The distribution of the chain end location (top) and schematic illustration of the chains (bottom) for $L/a = 100$ chains. (a) The L_{\parallel} lamellar phase, and (b) the L_{\perp} lamellar phase are shown separately for flat ($R = 0$) and corrugated ($R = 0.1d_0$) substrates.

larger than S_{\perp} , leading to a decrease in δS as the surface roughness amplitude R increases.

Figure 4c shows the case of the rigid chain ($L/a = 2$). As R/d_0 increases, δF decreases and δS increases, which is *completely opposite* to the behavior of Gaussian chains ($L/a = 100$). Such behavior is closely related to the chain configurations for small L/a . Figure 6 presents the calculated distribution of the chain ends for $L/a = 2$. Figure 6a shows that for the L_{\parallel} phase, the chain ends slide down into the valleys when BCPs are cast on top of a corrugated substrate. However, the polymer chains retain their standing-up configuration when they are cast on a flat substrate. By contrast, for the L_{\perp} orientation, figure 6b shows that the chain ends of the A-block concentrate in the middle of the thin film, indicating that the entire BCP chains stand up because the chains behave as rigid rods. As a consequence, increasing R enhances the chain configuration distortion of the L_{\perp} phase because the chains lie parallel to the flat surface, leading to a markedly decrease in the S_{\perp} entropy. Thus, the decrease of S_{\parallel} is smaller than in S_{\perp} , and $\delta S = S_{\parallel} - S_{\perp}$ increases with R . Consequently, δF decreases, indicating that the relative stability of L_{\perp} decreases.

BCP chains of $L/a = 5$, shown in figure 4b, manifest an intermediate behavior. As two different tendencies compete with each other, δS and δF nearly do not vary with R . Thus,

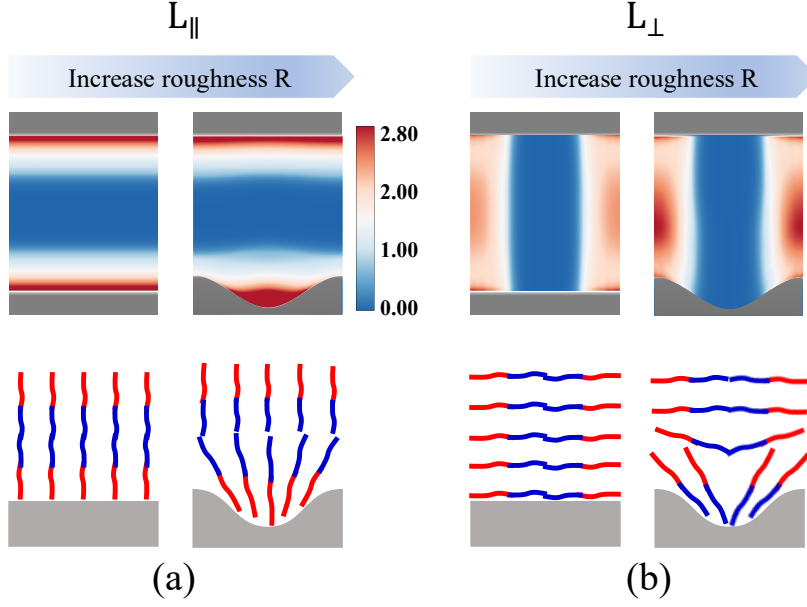


FIG. 6. The distribution of the chain-end location (top) and schematic illustration of the chains (bottom) for $L/a=2$ chains. (a) The L_{\parallel} lamellar phase, and (b) the L_{\perp} lamellar phase are shown separately for flat ($R=0$) and corrugated ($R=0.1d_0$) substrates.

the relative stability of the two phases does not change.

The self-assembly behavior of BCP thin films made of flexible chains (large L/a) is consistent with previous SCFT calculations,²⁵ where it was found that rough substrates can enhance the stability of the L_{\perp} phase. However, in the present study, we show that the response to the substrate roughness of rigid BCPs having a small L/a is opposite to that of long Gaussian chains. In the latter case, large surface roughness destabilizes the stability of the L_{\perp} phase, and there is a tendency for the L_{\perp} phase to undergo a transition into an L_{\parallel} one.

We note that the accurate quantitative comparison between the different behavior of rigid and Gaussian chains is the main finding of our study. Such findings have not been previously reported either in analytical works or in numerical simulations. These predictions should be verified in future experiments.

The dependence of the L_{\perp} -to- L_{\parallel} phase transition on the Substrate preference

As mentioned above, the substrate preference u is an important parameter to consider in tuning the L_{\perp} -to- L_{\parallel} phase transition, especially for BCP with high χ and low N , whose constituent blocks usually have considerably different surface energies. We keep the top surface neutral and flat while fixing the corrugation periodicity, $L_x = L_s = d_0$, of the bottom substrate. We then investigate the dependence of u^* , the critical value of the substrate preference, on the amplitude value R , where u^* is the critical value leading to the L_{\perp} -to- L_{\parallel} phase transition on the amplitude value R .

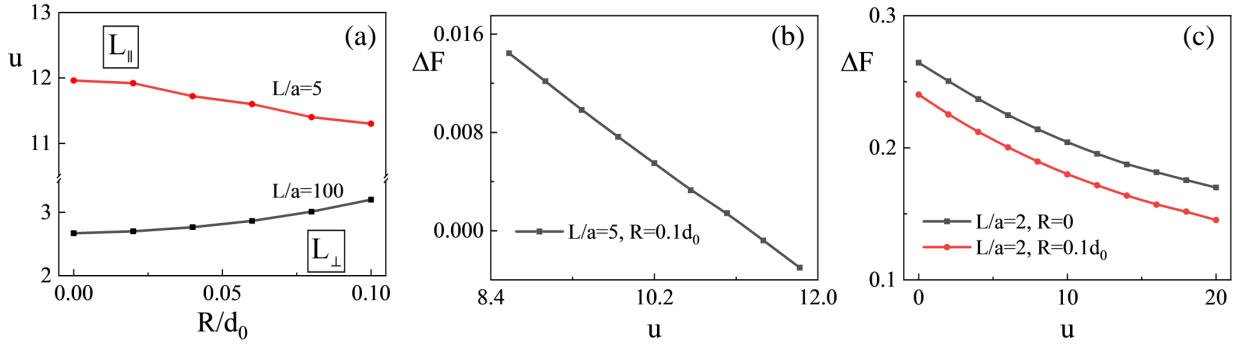


FIG. 7. (a) The L_{\perp} -to- L_{\parallel} phase diagram in the (u, R) plane, for two chain flexibilities: $L/a = 100$ (black line), and $L/a = 5$ (red line). (b) The dependence of $\Delta F = F_{\parallel} - F_{\perp}$ on the substrate preference u for $L/a = 5$ for roughness amplitude $R = 0.1d_0$. (c) The dependence of $\Delta F = F_{\parallel} - F_{\perp}$ on the substrate preference u for $L/a = 2$. The flat surface ($R = 0$) is denoted by a black line and the corrugate one ($R = 0.1d_0$) by a red line.

Figure 7a shows the phase transition (L_{\perp} -to- L_{\parallel}) between the perpendicular and parallel orientations in terms of the rescaled amplitude, R/d_0 , and the substrate preference, u . Any combination of u and R/d_0 values above the plotted transition line induces an L_{\perp} -to- L_{\parallel} phase transition. We show an example for $L/a = 5$ and $R/d_0 = 0.1$ in figure 7b. The value of ΔF changes from being positive to negative, indicating that a phase transition from L_{\perp} to L_{\parallel} occurs with the increase of u .

In addition, one can see in figure 7a that Gaussian chains having large $L/a = 100$, the critical value, u^* , corresponding to the L_{\perp} -to- L_{\parallel} phase transition, increases as a function of R/d_0 . For Gaussian polymers, the L_{\perp} phase becomes more stable as the substrate roughness increases. Therefore, larger surface preference is needed to induce the L_{\perp} -to- L_{\parallel} phase tran-

sition for larger substrate roughness. However, in the case of semi-flexible chains ($L/a = 5$), there is a slight negative correlation that u^* decreases as R/d_0 increases. The reason is that the L_{\perp} becomes less stable as R increases for semi-flexible and rigid polymers, resulting in a decrease of u^* . For rigid chains ($L/a = 2$), we do not find any meaningful value of u that can induce the L_{\perp} -to- L_{\parallel} phase transition. Furthermore, large u weakens the relative stability of the L_{\perp} as compared with L_{\parallel} . As shown in figure 7c, ΔF of $L/a = 2$ case decreases as u increases. This result means that increasing u and R are both favoring the L_{\parallel} phase for rigid polymers, but the effect is not strong enough to stabilize the L_{\parallel} phase as compared with the L_{\perp} phase.

CONCLUSIONS

We explore the self-assembly of symmetric AB diblock copolymers (BCP) confined in a thin-film geometry. Using SCFT which is based on a continuum WLC model, we focus on the influence of the substrate structure and chemistry on the conformations of polymer chains with various flexibilities. We systematically studied the combined effect of the polymer chain flexibility parameterized by L/a , substrate roughness amplitude R , and the surface preference u on the relative stability between the parallel (L_{\parallel}) and perpendicular (L_{\perp}) lamellar phases. The effects of these parameters on the relative stability of the L_{\perp} phase are presented in figure 8.

The stability of the L_{\perp} orientation

Chain flexibility	Roughness $R \uparrow$	Surface preference $u \uparrow$
Rigid (small L/a)	\downarrow	\downarrow
Semi-flexible (intermediate L/a)	nearly unchanged	\downarrow
Flexible (Large L/a)	\uparrow	\downarrow

FIG. 8. The combined effect of the chain flexibility L/a , substrate roughness R , and surface preference u on the stability of the L_{\perp} orientation.

Our results show that for BCP films confined between two flat and neutral substrates,

the lamellae domains tend to orient in the L_{\perp} direction, and decreasing the polymer chain flexibility will intensify this effect. However, increasing the substrate roughness R has distinctively different effects on polymers of different flexibility. While for Gaussian polymer chains (large L/a), the stability of the L_{\perp} phase is enhanced, the stability of the L_{\perp} phase is weakened for rigid polymer chains (small L/a). We further show that as R , the substrate roughness, increases, the critical value of the substrate preference, u^* , corresponding to the L_{\perp} -to- L_{\parallel} orientational transition decreases for rigid chains but increases for Gaussian chains. Such an opposite effect of substrate roughness for rigid chain polymers as compared to flexible ones was not observed in previous works and is one of our main results.

The origin of the distinctive behavior for Gaussian and semi-flexible (or rigid) BCP chains is obtained by analyzing the entropy and enthalpy contributions to the free energy. For Gaussian polymer chains, the roughness of the substrate influences more the conformational entropy of BCP chains in the L_{\parallel} as compared with the L_{\perp} due to the chain flexibility. Thus, the L_{\perp} stability is enhanced. Nevertheless, for rigid polymer chains, large roughness amplitude, R , affects more the chain conformational entropy in the L_{\perp} than in the L_{\parallel} due to the chain rigidity. Therefore, the effects of surface roughness on polymer conformational entropy weaken the L_{\perp} stability for rigid BCPs.

In conclusion, our study systematically manifests that rigid BCP chains (or short chains) are more likely to form an L_{\perp} phase in thin films, as is desirable in nano-lithography applications that are used to generate sub-10nm patterns. Using a corrugated substrate to induce a perpendicular orientation of the BCP film is useful for Gaussian BCP chains but will not work for rigid chains. We hope that our results may serve as a useful guide for future modeling experiments and applications.

Acknowledgement. This work was supported in part by the NSFC-ISF Research Program, jointly funded by the National Natural Science Foundation of China (NSFC) under grant No. 21961142020 and the Israel Science Foundation (ISF) under grant No. 3396/19, NSFC grants No. 21822302 and 22073004 and ISF grant No. 213/19, the Fundamental Research Funds for the Central University under grant No. YWF-22-K-101. We also ac-

knowledge the support of the High-Performance Computing Center of Beihang University.

REFERENCES

- [1] Sinturel, C.; Bates, F. S.; Hillmyer, M. A. High χ -low N block polymers: how far can we go? *ACS Macro Lett.* **2015**, *4*, 1044-1050.
- [2] Huang, C.; Zhu, Y.; Man, X. K. Block copolymer thin films. *Phys. Rep.* **2021**, *932*, 1-36.
- [3] Thurn-Albrecht, T.; Schotter, J.; Kastle, C. A.; Emley, N.; Shibauchi, T.; Krusin-Elbaum, L.; Guarini, K.; Black, C. T.; Tuominen, M. T.; Russell, T. P. Ultrahigh-density nanowire arrays grown in self-assembled diblock copolymer templates. *Science* **2000**, *290*, 2126-2129.
- [4] Park, C.; Yoon, J.; Thomas, E. L. Enabling nanotechnology with self-assembled block copolymer patterns. *Polymer* **2003**, *44*, 6725-6760.
- [5] Bates, F. S.; Schulz, M. F.; Khandpur, A. K.; Förster, S.; Rosedale, J. H.; Almdal, K.; Mortensen, K. Fluctuations, conformational asymmetry and block copolymer phase behaviour. *Faraday Discuss.* **1994**, *98*, 7-18.
- [6] Li, W.; Liu, M.; Qiu, F.; Shi, A.-C. Phase diagram of diblock copolymers confined in thin films. *J. Phys. Chem. B* **2013**, *117*, 5280-5288.
- [7] Bates, F. S.; Fredrickson, G. H. Block copolymers-designer soft materials. *Phys. Today* **1999**, *52*, 32-38.
- [8] Lee, Y.; Gomez, E. D. Challenges and opportunities in the development of conjugated block copolymer for photovoltaics. *Macromolecules* **2015**, *48*, 7385-7395.
- [9] Gu, K.; Loo, L. The polymer physics of multiscale charge transport in conjugated systems. *J. Polym. Sci. Part B: Polym. Phys.* **2019**, *57*, 1559-1571.
- [10] Peng, J.; Han, Y.-C. Recent advances in conjugated polythiophene-based rod-rod block copolymers: From morphology control to optoelectronic applications. *Giant* **2020**, *4*, 100039.
- [11] Cheng, J. Y.; Ross, C. A.; Chan, V. Z. H.; Thomas, E. L.; Lammertink, R. G. H.; Vancso, G. J. Formation of a cobalt magnetic dot array via block copolymer lithography. *Adv. Mater.* **2001**, *13*, 1174-1178.
- [12] Bates, C. M.; Maher, M. J.; Janes, D. W.; Ellison, C. J.; Willson, C. G. Block copolymer lithography. *Macromolecules* **2014**, *47*, 2-12.

- [13] Jung, Y. S.; Chang, J. B.; Verploegen, E.; Berggren, K. K.; Ross, C. A. A path to ultranarrow patterns using self-assembled lithography. *Nano Lett.* **2010**, *10*, 1000-1005.
- [14] Chaudhari, A.; Ghoshal, T.; Shaw, M. T.; Cummins, C.; Borah, D.; Holmes, J. D.; Morris, M. A. Formation of sub-7 nm feature size PS-b-P4VP block copolymer structures by solvent vapor process. *Proc. SPIE* **2014**, 905110.
- [15] Wang, C.; Li, X.; Deng, H. Synthesis of a fluoromethacrylate hydroxystyrene block copolymer capable of rapidly forming sub-5 nm domains at low temperatures. *ACS Macro Lett.* **2019**, *8*, 368-373.
- [16] Ding, S.; Zhang, Z.; Ye, Z.; Du, B.; Xu, J. Fabrication of high χ -low N block copolymers with thermally stable sub-5 nm microdomains using polyzwitterion as a constituent block. *ACS Macro Lett.* **2021**, *10*, 1321-1325.
- [17] J. Z. Y. Chen. Theory of wormlike polymer chains in confinement. *Progress in Polymer Science* **2016**, *54*, 3-46.
- [18] M. W. Matsen. Melts of semiflexible diblock copolymers. *J. Chem. Phys.* **1996**, *104*, 7758-7764.
- [19] Jiang, Y.; Chen, J. Z. Y. Self-consistent field theory and numerical scheme for calculating the phase diagram of worm-like diblock copolymers. *Phys. Rev. E* **2013**, *88*, 042603.
- [20] Jiang, Y.; Chen, J. Z. Y. Influence of chain rigidity on the phase behavior of wormlike diblock copolymers. *Phys. Rev. Lett.* **2013**, *110*, 138305.
- [21] Jiang, Y.; Zhang, W. Y.; Chen, J. Z. Y. Dependence of the disorder-lamellar stability boundary of a melt of asymmetric wormlike AB diblock copolymers on the chain rigidity. *Phys. Rev. E* **2011**, *84*, 041803.
- [22] Aissou, K.; Mumtaz, M.; Fleury, G.; Portale, G.; Navarro, C.; Cloutet, E.; Brochon, C.; Ross, C. A.; Hadzioannou, G. Sub-10 nm features obtained from directed self-assembly of semicrystalline polycarbosilane-based block copolymer thin films. *Adv. Mater.* **2015**, *27*, 261-265.
- [23] Suh, H. S.; Kim, D. H.; Moni, P.; Xiong, S.; Ocola, L. E.; Zaluzec, N. J.; Gleason, K. K.; Nealey, P. F. Sub-10-nm patterning via directed self-assembly of block copolymer films with a vapour-phase deposited topcoat. *Nat. Nanotechnol.* **2017**, *12*, 575-581.
- [24] Shin, D. O.; Lee, D. H.; Moon, H.-S.; Jeong, S.-J.; Kim, J. Y.; Mun, J. H.; Cho, H.; Park, S.; Kim, S. O. Sub-nanometer level size tuning of a monodisperse nanoparticle array via block

- copolymer lithography. *Adv. Funct. Mater.* **2011**, *21*, 250-254.
- [25] Man, X. K.; Tang, J. Z.; Zhou, P.; Yan, D. D.; Andelman, D. Lamellar diblock copolymers on rough substrates: self-consistent field theory studies. *Macromolecules* **2015**, *48*, 7689-7697.
- [26] Man, X. K.; Zhou, P.; Tang, J.; Yan, D. D.; Andelman, D. Defect-free perpendicular diblock copolymer films: the synergistic effect of surface topography and chemistry. *Macromolecules* **2016**, *49*, 8241-8248.
- [27] Zhu, Y.; Aissou, K.; Andelman, D.; Man, X. K. Orienting cylinder-forming block copolymer thin films: the combined effect of substrate corrugation and its surface energy. *Macromolecules* **2019**, *52*, 1241-1248.
- [28] Huang, H.; Liu, R.; Ross, C. A.; Alexander-Katz, A. Self-directed self-assembly of 3D tailored block copolymer nanostructures. *ACS Nano* **2020**, *14*, 15182-15192.
- [29] Tsori, Y.; Andelman, D. Parallel and perpendicular lamellae on corrugated surfaces. *Macromolecules* **2003**, *36*, 8560-8566.
- [30] Tsori, Y.; Sivaniah, E.; Andelman, D.; Hashimoto, T. Orientational transitions in symmetric diblock copolymers on rough surfaces. *Macromolecules* **2005**, *38*, 7193-7196.
- [31] Turner, M. S.; Joanny, J.-F. Diblock copolymer lamellae at rough surfaces. *Macromolecules* **1992**, *25*, 6681-6689.
- [32] Sivaniah, E.; Hayashi, H.; Iino, M.; Hashimoto, T.; Fukunaga, K. Observation of perpendicular orientation in symmetric diblock copolymer thin films on rough substrates. *Macromolecules* **2003**, *36*, 5894-5896.
- [33] Sivaniah, E.; Hayashi, H.; Matsubara, S.; Kiyono, S.; Hashimoto, T.; Fukunaga, K.; Kramer, E. J.; Mates, T. Symmetric diblock copolymer thin films on rough substrates. kinetics and structure formation in pure block copolymer thin films. *Macromolecules* **2005**, *38*, 1837-1849.
- [34] Kim, T.; Wooh, S.; Son, J. G.; Char, K. Orientation control of block copolymer thin films placed on ordered nanoparticle monolayers. *Macromolecules* **2013**, *46*, 8144-8151.
- [35] Sherck, N.; Webber, T.; Brown, D. R.; Keller, T.; Barry, M.; DeStefano, A.; Jiao, S.; Segalman, R. A.; Fredrickson, G. H.; Shell, M. S.; Han, S. End-to-end distance probability distributions of dilute poly(Ethylene Oxide) in aqueous solution. *J. Am. Chem. Soc.* **2020**, *42*, 19631-19641.
- [36] Scott P. O. Danielsen, Colin R. Bridges, and Rachel A. Segalman. Chain stiffness of donor-acceptor conjugated polymers in solution. *Macromolecules* **2022**, *55*, 437-449.
- [37] Kratky, O.; Porod, G. Röntgenuntersuchung gelöster Fadenmoleküle. *Recl. Trav. Chim. Pays-*

- Bas* **1949**, 68, 1106-1122.
- [38] Matsen, M. W. Self-Consistent field theory for melts of low-molecular-weight diblock copolymer. *Macromolecules* **2012**, 45, 8502-8509.
 - [39] Jiang, Y.; Zhang, X.; Miao, B.; Yan, D.; Chen, J. Z. Y. Microphase separation of short wormlike diblock copolymers with a finite interaction range. *Soft Matter* **2016**, 12, 2481-2490.
 - [40] Saito, N.; Takahashi, K.; Yunoki, Y. The statistical mechanical theory of stiff chains. *J. Phys. Soc. Jpn.* **1967**, 22, 219-226.
 - [41] Spakowitz, A. J.; Wang, Z.-G. End-to-end distance vector distribution with fixed end orientations for the wormlike chain model. *Phys. Rev. E* **2005**, 72, 041802.
 - [42] M. W. Matsen. Thin films of block copolymer. *J. Chem. Phys.* **1997**, 106, 7781.
 - [43] Bosse, A. W.; García-Cervera, C. J.; Fredrickson, G. H. Microdomain ordering in laterally confined block copolymer thin films. *Macromolecules* **2007**, 40, 9570-9581.
 - [44] Fredrickson, G. H. *The Equilibrium Theory of Inhomogeneous Polymers*; Oxford University Press, New York, 2006.
 - [45] Hur, S.-M.; García-Cervera, C. J.; Kramer, E. J.; Fredrickson, G. H. SCFT simulations of thin film blends of block copolymer and homopolymer laterally confined in a square well. *Macromolecules* **2009**, 42, 5861-5872.
 - [46] Takahashi, H.; Laachi, N.; Delaney, K. T.; Hur, S.-M.; Weinheimer, C. J.; Shykind, D.; Fredrickson, G. H. Defectivity in laterally confined lamella-forming diblock copolymers: thermodynamic and kinetic aspects. *Macromolecules* **2012**, 45, 6253-6265.
 - [47] Dalsin, S. J.; Rions-Maehren, T. G.; Beam, M. D.; Bates, F. S.; Hillmyer, M. A.; Matsen, M. W. Bottlebrush block polymers: quantitative theory and experiments. *ACS Nano* **2015**, 9, 12233-12245.
 - [48] Paturej, J.; Sheiko, S. S.; Panyukov, S.; Rubinstein, M. Molecular structure of bottlebrush polymers in melts. *Sci. Adv.* **2016**, 2, e1601478.
 - [49] Gettinger, C. L.; Heeger, A. J.; Drake, J. M.; Pine, D. J. A photoluminescence study of poly(phenylene vinylene) derivatives: the effect of intrinsic persistence length. *J. Chem. Phys.* **1994**, 101, 1673-1678.
 - [50] McCulloch, B.; Ho, V.; Hoarfrost, M.; Stanley, C.; Do, C.; Heller, W. T.; Segalman, R. A. Polymer Chain shape of poly(3-alkylthiophenes) in solution using small-angle neutron scattering. *Macromolecules* **2013**, 46, 1899-1907.

- [51] Fei, H.-F.; Yavitt, B. M.; Hu, X.; Kopanati, G.; Ribbe, A.; Watkins, J. J. Influence of molecular architecture and chain flexibility on the phase map of polystyrene-block-poly(dimethylsiloxane) brush block copolymers. *Macromolecules* **2019**, *52*, 6449-6457.
- [52] Feng, X.; Nejati, S.; Cowan, M. G.; Tousley, M. E.; Wiesenauer, B. R.; Noble, R. D.; Elimelech, M.; Gin, D. L.; Osuji, C. O. Thin polymer films with continuous vertically aligned 1 nm pores fabricated by soft confinement. *ACS Nano* **2016**, *10*, 150-158.
- [53] Pickett, G. T.; Witten, T. A.; Nagel, S. R. Equilibrium surface orientation of lamellae. *Macromolecules* **1993**, *26*, 3194-3199.
- [54] Pickett, G. T.; Balazs, A. C. Equilibrium orientation of confined diblock copolymer films. *Macromolecules* **1997**, *30*, 3097-3103.
- [55] Chen, J. Z. Y.; Sullivan, D. E. Free energy of a wormlike polymer chain confined in a slit: crossover between two scaling regimes. *Macromolecules* **2006**, *39*, 7769-7773.

for Table of Contents use only

The Chain Flexibility Effects on the Self-assembly of Diblock Copolymer in Thin Film

Mingyang Chen, Yuguo Chen, Yanyan Zhu, Ying Jiang, David Andelman*, and Xingkun Man**

The stability of perpendicular lamellar phase:

